

Study of Active Negative Group Delay Circuit Based on LNA and RLC-Parallel Network

Dan Chen¹, Taochen Gu², Xiang Zhou³, Fayu Wan^{2, *}, and Blaise Ravelo²

Abstract—This paper develops a circuit theory on bandpass negative group delay (NGD) topology. The NGD active lumped circuit uses a low noise amplifier (LNA). An S -parameter model is formulated. Unfamiliar, NGD function analysis is introduced by analytically defining the NGD value, bandwidth, and central frequency as a function of the topology parameters. The synthesis formulas enabling the calculation of cell parameters as a function of the targeted bandpass function specifications. To validate the circuit theory, an NGD proof of concept (PoC) is designed, simulated, and tested. As expected, simulations and measurements are in good agreement. Calculated model, simulated and measured results showing NGD level of about -10 ns around the centre frequency 0.5 GHz over the bandwidth 50 MHz validate are obtained.

1. INTRODUCTION

The first negative group delay (NGD) microwave devices were designed with passive circuits in 1990s [1]. In 2000s, NGD topologies inspired from left-handed metamaterial structures were developed [2]. A few years later, microwave distributed topologies generating NGD effect were introduced by exploiting electromagnetic coupling effects [3,4]. However, these passive NGD circuits operate inherently either with absorption or with strong reflections. Therefore, the application possibilities are very limited. Despite the systematic limitation inherently to the NGD function [5], different applications notably in the microwave engineering were proposed. For example, NGD function application to design high-performance feed forward amplifier and bandwidth enhancement was also proposed [6,7]. To face the NGD passive attenuation loss limitations, topologies of active microwave cells using field effect transistors (FETs) were investigated [8–9]. It was pointed that the NGD function presents behaviors like a classical filter [10]. Indeed, various classes of NGD function as low-pass, high-pass and bandpass NGDs were introduced [10]. It is noteworthy that the FET-based NGD microwave topologies require further improvement on the access-matching and biasing networks design complexity. Furthermore, FET-based NGD circuits present a systematical sign inversion of output voltage compared to the input. To overcome the bias and access matching network design complexity, NGD topologies were proposed replacing the FET by low noise amplifier (LNA) [11–15]. The alternative LNA-based NGD topology is expected to present considerable advantages like design simplicity. This active topology is prominent to achieve better access matching and allowing to avoid the instability. We address further understand of NGD function in the present paper.

The NGD theory developed in the present paper is quite easy to understand for non-specialist microwave engineers. The paper explains theoretical and experimental approaches of a bandpass NGD active topology. Difference from the NGD topology presented in [11], the proposed one is established

Received 31 December 2020, Accepted 18 February 2021, Scheduled 26 February 2021

* Corresponding author: Fayu Wan (fayu.wan@gmail.com).

¹ State Key Laboratory of Nuclear Power Safety Monitoring Technology and Equipment, Shenzhen 518172, China. ² Nanjing University of Information Science & Technology (NUIST), Nanjing, Jiangsu 210044, China. ³ Southeast University, Nanjing, Jiangsu 210044, China.

from a lumped element components-based RC parallel network. For better comprehension, it is mainly divided in three main sections:

- Section 2 is focused on the theoretical NGD analysis. The NGD bandpass cell is a first order circuit. The S -parameter model is briefly introduced.
- Section 3 is focused on the NGD analysis and characterization.
- Section 4 describes the experimental validations compared to analytical modelling and simulations of the proposed LNA-based NGD topology.
- Lastly, Section 5 draws the conclusion.

2. TOPOLOGICAL DEFINITION OF THE BANDPASS NGD ACTIVE CIRCUIT UNDER STUDY

The topology of the bandpass NGD active cell is introduced. The NGD analysis is developed from S -parameter modelling. The synthesis equations are established in function of the targeted NGD function.

2.1. Definition of Bandpass NGD Function

Acting as a two-port system, by denoting ω the variable angular frequency, an NGD circuit S -matrix can be written as:

$$[S(j\omega)] = \begin{bmatrix} S_{11}(j\omega) & S_{12}(j\omega) \\ S_{21}(j\omega) & S_{22}(j\omega) \end{bmatrix} \quad (1)$$

To analyse the NGD function, we need the magnitude of transmission ($p \neq q$) and reflection ($p = q$) coefficients, respectively:

$$S_{pq}(\omega) = |S_{pq}(j\omega)| \quad (2)$$

with $p, q = \{1, 2\}$. GD is analytically defined by:

$$\tau(\omega) = -\frac{\partial \varphi(\omega)}{\partial \omega} \quad (3)$$

by reminding that the transmission phase:

$$\varphi(\omega) = \angle S_{21}(j\omega). \quad (4)$$

The graphical specification of bandpass NGD function is shown in Fig. 1, with centre angular frequency ω_0 , cut-off angular frequencies $\omega_{c1,2}$, and negative angular frequencies $\omega_{n1,2}$ which are defined by:

$$\begin{cases} \tau(\omega_{c1,2}) = 0 \\ \tau(\omega_{n1,2}) = \tau_0 < 0 \end{cases} \quad (5)$$

The NGD bandwidth (BW) [10] is given by:

$$\Delta\omega = \omega_{c2} - \omega_{c1}. \quad (6)$$

Acting as an RF/microwave function, the GD specification must be associated with the transmission gain flatness $G_a \leq S_{21}(\omega) \leq G_b$ in the NGD bandwidth $\omega_{c1} \leq \omega \leq \omega_{c2}$.

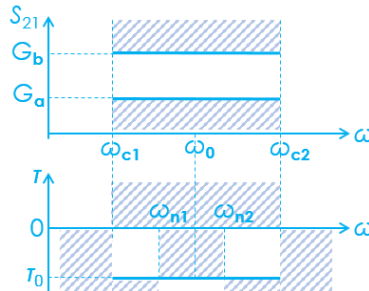


Figure 1. Typical specification of bandpass NGD function magnitude and GD.

2.2. General Description of the LNA-Based Topology

The general topology adopted in the present study is depicted in Fig. 2. It consists of an LNA with upstream and downstream connected series impedances Z .

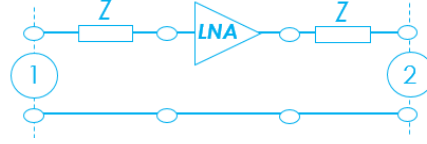


Figure 2. General topology of the LNA based active cell under study.

The LNA is assumed as a non-unilateral ($S_{12} \neq 0$) and defined by the S -parameter model:

$$[S^{LNA}(j\omega)] = \begin{bmatrix} r & r \\ t & r \end{bmatrix} \tag{7}$$

with t and r being the LNA transmission, and reflection and isolation coefficients. In the considered operating bandwidth, these coefficients are assumed constant and independent of the frequency variables.

2.3. Global S -Matrix Model

As represented in Fig. 3, the equivalent S -matrix of the topology introduced in Fig. 2 can be determined by considering the S -matrix of each constituting block $[S^{LNA}]$ and:

$$[S^Z(j\omega)] = \frac{1}{Z(j\omega) + 2R_0} \begin{bmatrix} Z(j\omega) & 2R_0 \\ 2R_0 & Z(j\omega) \end{bmatrix}. \tag{8}$$

The total transfer matrix can be easily determined knowing the circuit and system theory [11, 12]. Indeed, it is equal to the matrix product between the cascaded constituting cells. The global S -matrix can be derived from the transfer matrix of the overall circuit:

$$S_{11}(j\omega) = S_{22}(j\omega) = \frac{r^2 Z(j\omega) [Z(j\omega) - R_0] + 4rR_0^2 - r(t + 2)Z^2(j\omega) + 2(1 + r t)R_0 Z(j\omega)}{[(1 - r)Z(j\omega) + 2R_0]^2} \tag{9}$$

$$S_{12}(j\omega) = \frac{4rR_0^2}{[(1 - r)Z(j\omega) + 2R_0]^2} \tag{10}$$

$$S_{21}(j\omega) = \frac{4R_0^2 t}{[(1 - r)Z(j\omega) + 2R_0]^2}. \tag{11}$$

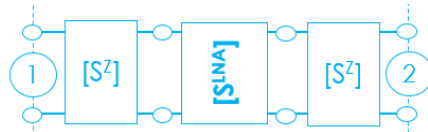


Figure 3. S -matrix diagram equivalent to the topology introduced in Fig. 2.

3. NGD ANALYSIS WITH AND RLC-NETWORK BASED CELL

An example of bandpass NGD cell is elaborated in the present section. The main NGD properties are analytically defined in the function of circuit parameters.

3.1. Introduction of the Lumped RLC Network Cell

Among the simplest circuits allowing to fulfil the bandpass NGD specified in Fig. 1, we can choose the series impedance Z as constituted by an RLC-parallel passive network. Therefore, our LNA based topology is transformed into the schematic shown in Fig. 4.

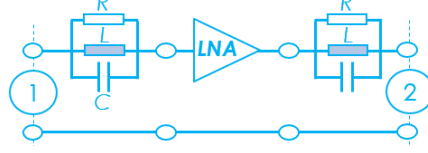


Figure 4. RLC passive network and LNA based cell.

Under the configuration of RLC-parallel network impedance shown in Fig. 4, the series impedance Z is analytically given by:

$$Z(j\omega) = \frac{j\omega RL}{R(1 - LC\omega^2) + j\omega RL} \quad (12)$$

3.2. NGD Analysis

The NGD analysis consists in determining the properties between the circuit parameters to realize the inequality:

$$\tau(\omega) < 0 \quad (13)$$

in the NGD bandwidth $\omega_{c1} \leq \omega \leq \omega_{c2}$. To perform this analysis, we can consider the S -matrix and GD at the particular frequency:

$$\omega_0 = \frac{1}{\sqrt{LC}} \quad (14)$$

By means of Eq. (3), the S -parameter at the resonance frequency can be rewritten as:

$$S_{11}(\omega_0) = S_{22}(\omega_0) = \frac{r(r - t - 2)R^2 + 4rR_0^2 + R_0R(2 + rt - r^2)}{[(1 - r)R + 2R_0]^2} \quad (15)$$

$$S_{12}(\omega_0) = \frac{4rR_0^2}{[(1 - r)R + 2R_0]^2} \quad (16)$$

$$S_{21}(\omega_0) = \frac{4tR_0^2}{[(1 - r)R + 2R_0]^2}. \quad (17)$$

The GD at the center frequency can be written as:

$$\tau(\omega_0) = \frac{2(r - 1)R^2C}{(1 - r)R + 2R_0}. \quad (18)$$

3.3. Synthesis Method

The bandpass NGD cell synthesis consists in calculating the parameters R , L and C in function of the targeted reflection coefficient m , targeted transmission gain g , NGD level $\tau_0 < 0$, and the centre frequency ω_0 by means of equations related to:

- the transmission coefficient:

$$S_{21}(\omega_0) = g \quad (19)$$

- the GD:

$$\tau(\omega_0) = \tau_0 \quad (20)$$

- and the reflection coefficient:

$$S_{11}(\omega_0) = m. \quad (21)$$

The derived expressions of the bandpass cell resistance and inductance are written as:

$$R = \frac{2(\sqrt{t} - \sqrt{g})R_0}{\sqrt{g}(1-r)} \quad (22)$$

$$C = \frac{\tau_0(r-1)R}{2R[2R_0 + (1-r)R]}. \quad (23)$$

It is noteworthy that the resistance R exists only if:

$$g < t. \quad (24)$$

By inverting Equation (14), the inductance can be calculated from equation:

$$L = \frac{1}{C\omega_0^2}. \quad (25)$$

To check the bandpass NGD theory validity, the next section will describe the design, simulation, and experimental results. The proposed demonstrators are aimed to make the established theory as familiar as possible to non-specialists.

4. EXPERIMENTAL VALIDATION

This section is focused on the feasibility study of the bandpass NGD theory. The NGD circuits [1–13] are designed similarly to classical and familiar electronic microwave circuits by paying attention to the condition in Eq. (5). The PoC was designed and simulated in the ADS[®] commercial tool from Keysight Technologies[®].

4.1. PoC Description

The NGD circuit design and fabrication were carried out in two steps. First, the ideal circuit was designed and simulated following the synthesis formulas established previously. Then, the real circuit was fabricated in function of the available components and technology in our laboratory.

4.1.1. Ideal NGD Circuit Design

The NGD circuit design was started with an ideal circuit. The RLC lumped element values were calculated with the synthesis Equations (23), (24), and (26). The NGD circuit was intended to operate under the specifications $g = 0$ dB and $\tau(f_0) = -10$ ns with the NGD centre frequency $f_0 = 0.5$ GHz. Based on these specifications, the cartographies showing the variation of R , L , and C in function of couple (r, t) were established in Figs. 5(a), (b), and (c), respectively. These mappings were exploited to choose the adequate LNA in function of its reflection and transmission parameters to realize the NGD circuit.

After different comparisons of available LNA in the market, we choose the packed MMIC LEE-9+ from mini-circuits employed in [11, 12]. This LNA is specified by the transmission gain $t = 8.5$ dB and input/output reflection coefficient average value $r = -22$ dB. Then, the ideal bandpass NGD cell was calculated, and the chosen real parameters with 5% tolerances are addressed in Table 1.

Table 1. Ideal and chosen real NGD prototype parameters.

	R	C	L
Ideal	68.56 Ω	94.23 pF	1.07 nH
Real	68 Ω	95 pF	1.07 nH

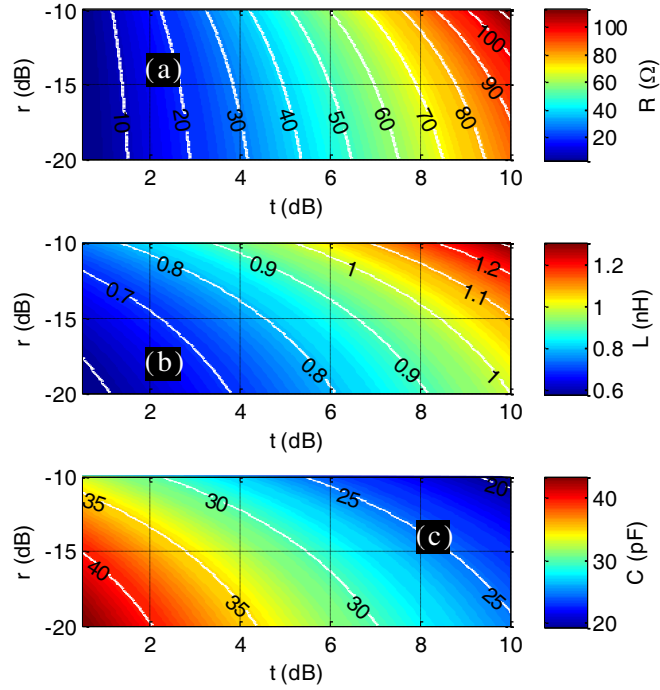


Figure 5. Mappings of (a) R , (b) L and (c) C versus the LNA reflection and transmission coefficients.

4.1.2. NGD Prototype Implementation

Figure 6(a) highlights the detailed schematic of the LNA based designed circuit. The bias and decoupling circuits are indicated in thin lines. The RF/microwave parts are indicated in bold lines. Fig. 6(b) represents a photo of the fabricated circuit prototype which was implemented in hybrid technology. The lumped passive elements were chosen by using commercially available surface mounted components (SMCs).

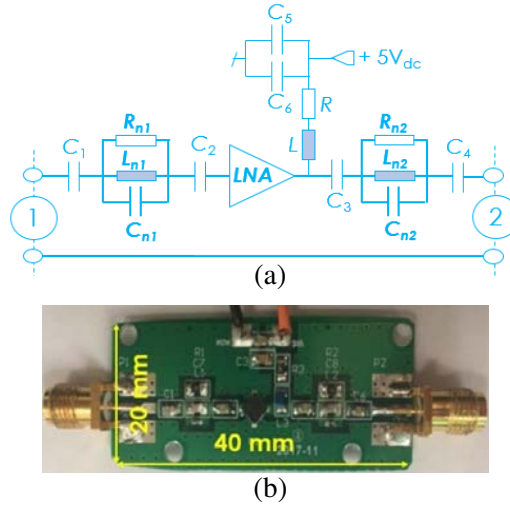


Figure 6. Photograph of the fabricated NGD prototype ($R_{n1} = R_{n2} = 68\ \Omega$, $L_{n1} = L_{n2} = 1.1\ \text{nH}$, $C_{n1} = C_{n2} = 95\ \text{pF}$, $R = 22\ \Omega$, $L = 5\ \text{mH}$, $C_1 = C_2 = C_3 = C_4 = 10\ \mu\text{F}$, $C_5 = 100\ \text{nF}$, $C_6 = 10\ \text{nF}$).

The printed circuit board was implemented on an FR4 epoxy dielectric substrate. The geometrical and physical characteristics of the substrate are addressed in Table 2.

Table 2. Fabricated circuit substrate parameters.

Constituting element	Designation	Parameters	Values
Substrate	Dielectric substrate thickness	h	1.6 mm
	Relative permittivity	ϵ_r	4.4
	Metallization thickness	t	35 μm
	Loss tangent	$\tan(\delta)$	0.12
	Metallization conductivity	σ	58 MS/m

4.2. Discussion on Simulation and Measurement Results

The experimental validation of the bandpass NGD PoC was carried out with S -parameter measurements. The tested S -parameters are measured with Vector Network Analyzer (VNA) from Rohde & Schwarz[®] which presents the reference ZNB 20, frequency band 100 kHz to 20 GHz.

The present S -parameter analyses were performed from 0.35 GHz to 0.7 GHz. Figs. 7(a) and 7(b) display the comparisons of modelled, simulated, and measured GDs and transmission coefficients, respectively. The experimental results are in good agreement with the theory and simulation. As predicted by our theory, the measured results correspond to the bandpass NGD responses. Emphatically, theoretical models, simulations, and experimentations confirm that the LNA-based bandpass NGD topology introduced in Fig. 1 operates as a bandpass NGD function.

The tested prototype exhibits an NGD central frequency around 0.5 GHz, NGD level -10 ns over the bandwidth 50 MHz. In addition to the NGD aspect validation, the NGD prototypes generate transmission gain slightly more than 0 dB. As illustrated in Figs. 8(a) and 8(b), the input and output reflection coefficients are better than -9 dB. The relative differences between the simulated and experimental results, especially seen around the NGD centre frequency about 20% are mainly due to the used component tolerances and the LNA model defined in matrix expression (25). The slight

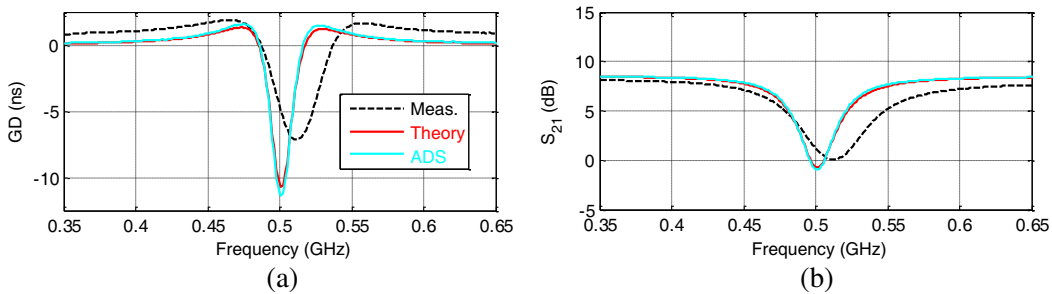


Figure 7. (a) GD and (b) transmission parameter of the bandpass NGD circuit.

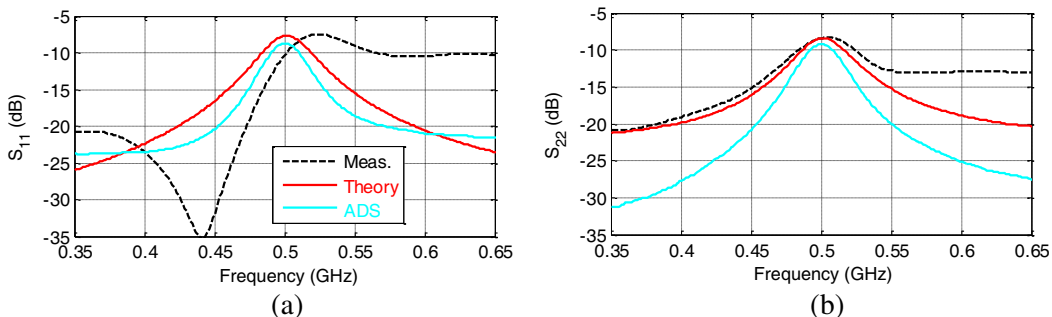


Figure 8. (a) Input and (b) output reflection coefficients of the bandpass NGD circuit.

differences between the simulations and measurements may be mainly caused by the dielectric substrate permittivity dispersion and the circuit fabrication imperfection, and the obtained results are in good correlation in the centre frequency.

4.3. Application of BP NGD

The potential applications of the bandpass NGD circuit proposed are:

- a. RF/microwave phase shifters: The bandpass NGD active circuits were also applied to design an innovative type of phase shifter. The NGD phase shifter design principle is based on cascading the positive group delay and NGD circuit. The technique was exploited to design a phase equalizer making use of negative group delay times by reflection coefficients. The technique was developed to synthesize a broadband-independent frequency phase shifter.
- b. Microwave and digital signal delay reduction: The NGD could be an equalization technique of signal propagation. It was applied to high speed metamaterial-inspired NGD CMOS circuits. Then, by using an FET based NGD active circuit, the technique was extended to the PCB electrical interconnect effect equalization for the signal integrity enhancement.

5. CONCLUSION

A bandpass NGD microwave theory of LNA based topology is developed. The active cell S -parameter model was established in order to make the NGD analysis. The characteristics of the bandpass NGD function as NGD level, center frequency, bandwidth, transmission gain, and reflection coefficient are analytically expressed. The NGD active cell parameter formulas are given in function of targeted the NGD specifications.

The established NGD circuit theory is validated with comparisons among the calculated model, simulations with ADS[®], and measurements. As PoC, a hybrid prototype was designed, simulated, fabricated, and tested. As expected in theory, calculated, simulated and measured NGD and S -parameter results are in very good agreement.

ACKNOWLEDGMENT

This research work was supported in part by NSFC under Grant 61971230, and in part by Jiangsu Specially Appointed Professor program and Six Major Talents Summit of Jiangsu Province (2019-DZXX-022) and in part by the Startup Foundation for Introducing Talent of NUIST, in part by the Postgraduate Research & Practice Innovation Program of Jiangsu Province under Grant KYCX20_0966.

REFERENCES

1. Lucyszyn, S., I. D. Robertson, and A. H. Aghvami, "Negative group delay synthesizer," *Electronics Letters*, Vol. 29, No. 9, 798–800, Apr. 1993.
2. Siddiqui, O. F., M. Mojahedi, and G. V. Eleftheriades, "Periodically loaded transmission line with effective negative refractive index and negative group velocity," *IEEE Trans. Antennas Propagat.*, Vol. 51, No. 10, 2619–2625, Oct. 2003.
3. Chaudhary, G. and Y. Jeong, "Tunable center frequency negative group delay filter using coupling matrix approach," *IEEE Microwave Wireless Component Letters*, Vol. 27, No. 1, 37–39, 2017.
4. Liu, G. and J. Xu, "Compact transmission-type negative group delay circuit with low attenuation," *Electronics Letters*, Vol. 53, No. 7, 476–478, Mar. 2017.
5. Kandic, M. and G. E. Bridges, "Asymptotic limits of negative group delay in active resonator-based distributed circuits," *IEEE Transactions on Circuits and Systems I: Regular Papers*, Vol. 58, No. 8, 1727–1735, Aug. 2011.
6. Choi, H., Y. Jeong, C. D. Kim, and J. S. Kenney, "Efficiency enhancement of feedforward amplifiers by employing a negative group delay circuit," *IEEE Trans. Microw. Theory Tech.*, Vol. 58, No. 5, 1116–1125, May 2010.

7. Choi, H., Y. Jeong, C. D. Kim, and J. S. Kenney, "Bandwidth enhancement of an analog feedback amplifier by employing a negative group delay circuit," *Progress In Electromagnetics Research*, Vol. 105, 253–272, 2010.
8. Ravelo, B., "Investigation on microwave negative group delay circuit," *Electromagnetics*, Vol. 31, No. 8, 537–549, Nov. 2011.
9. Wu, C.-T. M. and T. Itoh, "Maximally flat negative group delay circuit: A microwave transversal filter approach," *IEEE Trans. Microw. Theory Tech.*, Vol. 62, No. 6, 1330–1342, Jun. 2014.
10. Ravelo, B., "Similitude between the NGD function and filter gain behaviours," *Int. J. Circ. Theor. Appl.*, Vol. 42, No. 10, 1016–1032, Oct. 2014.
11. Wan, F., N. Li, B. Ravelo, Q. Ji, B. Li, and J. Ge, "The design method of the active negative group delay circuits based on a microwave amplifier and an RL-series network," *IEEE Access*, Vol. 6, 33849–33858, Dec. 2018.
12. Wan, F., J. Wang, B. Ravelo, J. Ge, and B. Li, "Time-domain experimentation of NGD active RC-network cell," *IEEE Trans. Circuits and Systems II: Express Briefs*, Vol. 66, No. 4, 562–566, Apr. 2019.
13. Wan, F., X. Miao, B. Ravelo, Q. Yuan, J. Cheng, Q. Ji, and J. Ge, "Design of multi-scale negative group delay circuit for sensors signal time-delay cancellation," *IEEE Sensors Journal*, Vol. 19, No. 19, 8951–8962, Oct. 2019.
14. Wan, F., Z. Yuan, B. Ravelo, J. Ge, and W. Rahajandraibe, "Low-pass NGD voice signal sensing with passive circuit," *IEEE Sensors Journal*, Vol. 20, No. 12, 6762–6775, Jun. 2020.
15. Wan, F., L. Wang, Q. Ji, and B. Ravelo, "Canonical transfer function of band-pass NGD circuit," *IET Circuits, Devices & Systems*, Vol. 13, No. 2, 125–130, Mar. 2019.